Eur. Phys. J. D **2**, 131–141 (1998)

THE EUROPEAN PHYSICAL JOURNAL D

Temporal coherent control induced by wave packet interferences in one and two photon atomic transitions

M.A. Bouchene[1], V. Blanchet[1,a], C. Nicole[1], N. Melikechi[1,b], B. Girard[1,c], H. Ruppe[2], S. Rutz[2], E. Schreiber[2,d], and L. Wöste[2]

[1] Laboratoire de Collisions Agrégats Réactivité, C.N.R.S.[e], IRSAMC, Université Paul Sabatier, 118 Route de Narbonne, 31062 Toulouse Cedex, France
[2] Freie Universität Berlin, Experimentalphysik, Arnimallee 14, 14169 Berlin, Germany

Received: 30 December 1997 / Revised: 28 February 1998 / Accepted: 4 March 1998

Abstract. The interaction of a sequence of two identical ultrashort laser pulses with an atomic system results in quantum interferences as in Ramsey fringes experiments. These interferences allow achievement of temporal coherent control of the excitation probability. We present the results of a temporal coherent control experiment on two different atomic systems: one-photon absorption in K ($4s-4p$) and two-photon absorption in Cs ($6s-7d$). In K, the quantum interferences between the two excitation paths associated with the laser pulses are revealed through rapid oscillations of the excitation probability as a function of the time delay between the two pulses. These oscillations take place at the transition frequency (period $T = 2.56$ fs). The interferences are modulated by beats (at about 580 fs) resulting from the doublet structure of the excited state ($4p$ ($^2P_{1/2}$, $^2P_{3/2}$)). Three complementary interpretations of this experiment are presented: in terms of beats of quantum interferences, of variation in the spectrum intensity, and of wave packet interferences. Whenever the two laser pulses are temporally overlapped, optical interferences are superimposed on to the quantum interferences. The distinction between these two types of interference is clearly revealed in the two-photon excitation scheme performed on Cs ($6s-7d$ ($^2D_{3/2}$, $^2D_{5/2}$)) because quantum interferences occur at twice the frequency of the optical interferences.

PACS. 32.80.Qk Coherent control of atomic interactions with photons – 32.80.Rm Multiphoton ionization and excitation to highly excited states (*e.g.*, Rydberg states) – 42.50.Md Optical transient phenomena: quantum beats, photon echo, free-induction decay, dephasings and revivals, optical nutation, and self-induced transparency

1 Introduction

Since its recent inception, laser control of molecular and chemical processes has been the subject of many theoretical and experimental efforts [1–4]. Optimal control is based on the design of tailored laser pulses that can create a wave packet able to reach the chosen target [3–10]. In active control, two ultrashort laser pulses are used to take advantage of the time evolution of the wave packet. One of the two laser pulses creates a wave packet while the second, slightly delayed in time, transfers this wave packet to the desired final state whenever it reaches the transition region [11–14]. Other schemes based on rapid adiabatic transition have been shown to yield high population transfer. Examples of these include Stimulated Raman Scattering with Adiabatic Passage (STIRAP) [15] or Laser Induced Continuum Structure (LICS) [16,17].

In coherent control experiments [2,18], interferences between two quantum pathways leading to the same final state, are used to govern the excitation probability of the system. In the most widely used scheme, interferences are created between a three-photon transition and a one-photon transition induced by two coherent optical fields [19–25]. The total cross-section of the excitation process can be controlled with a contrast close to 100% [24].

Differential cross-sections have also been controlled. Using interferences between two-photon and one-photon transitions, the groups of Bucksbaum and Elliott have reported control of the anisotropy of photoelectron angular distribution [26,27]. Furthermore, this technique has been successfully implemented to control fragments in

[a] *Present address:* Steacie Institute for Molecular Sciences, NRC, Ottawa Ont. K1A 0R6, Canada
[b] *Permanent address:* Department of Physics & Astronomy and Applied Optics Center, Delaware State University, Dover, DE 19901, USA
[c] Membre de l'Institut Universitaire de France
e-mail: `bertrand@yosemite.ups-tlse.fr`
[d] *Permanent address:* Max-Born-Institut für Nichtlineare Optik und Kurzzeitspektroskopie, Rudower Chaussee 6, 12474 Berlin, Germany
[e] UMR 5589

molecular photodissociation [28,29], photocurrents [30], and isotopic separation [29,31].

Temporal coherent control consists of using two identical frequencies to create, in the time domain, two quantum paths slightly delayed in time. This time delay is used to control the phase of the interference. This technique is similar to that developed for conducting Ramsey fringes measurements [32–34] although the method of observation of the fringes is different. In temporal coherent control experiments, the fringes are observed in the time domain [35–37], while in Ramsey fringes experiments, the fringes are observed in the frequency domain. This technique can be implemented using two identical ultrashort laser pulses [35,38–45] and indeed has already been used in many fields, to monitor the free evolution of an excited state wave packet. The contrast of the interference signal reflects the overlap between the free evolving wave packet and the initial wave packet. Such experiments have been conducted in Rydberg state wave packets [36,46–49], electronic spin wave packets [43], nuclear spin wave packets [44], exciton wave packets in quantum wells [50, 51], molecular wave packets in the gas phase [35,38,39, 45], and in the liquid phase [52]. These studies have not been restricted to the low field regime. In the high field regime, interferences have been observed between several multiphoton excitation paths [40]. However, the possibility of using this technique as a coherent control tool was overlooked until recently [39,41,42,45].

Observing the quantum interferences in temporal coherent control requires excellent stability of the delay lines. To keep the relative phase between the two laser pulses constant (within a multiple of 2π), phase locking has been used [35,38,52]. Information on the motion of the wave packet is contained in the envelope of the interferences. It can be directly extracted without recording the full interference pattern (interferogram) by using a phase sensitive detection technique [47–49,53] or simply by measuring the amplitude of the fluctuations resulting from random phase variations [54].

While most of the features of the temporal coherent control based on wave packet interferences have been widely discussed and understood [35,55–57], the relationship between quantum interferences and optical interferences has often been ignored. Similarly, the link between the temporal interpretation and the spectral interpretation have been also overlooked.

In this paper, we present a detailed comparison between interferences induced by one-photon and two-photon transitions in K and Cs atoms respectively. The quantum system is an electronic spin wave packet created in a fine structure doublet state. The linear response of the one-photon interference in the weak field regime provides several physical interpretations of the experiment. The two-photon transition experiment provides an unambiguous distinction between these two kinds of interferences [43]. Furthermore, the extension of the interpretations given for the one-photon interference to the two-photon case is discussed.

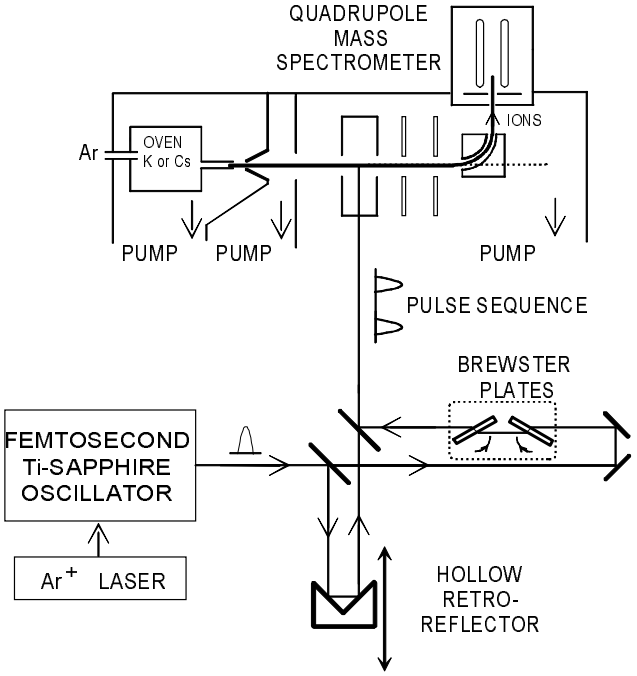

Fig. 1. Experimental setup: The laser beam crosses the atomic beam at right angle. Ions are detected at 90° in a quadrupole mass spectrometer. A femtosecond laser is splitted in two pulses. The optical delay between the two pulses is made by moving the retroreflector by 6.67 fs steps or by rotating a pair of Brewster Plates around a vertical axis allowing a 0.3 fs resolution scan.

A brief description of the experimental set-up is presented in Section 2. In Section 3, the three interpretations of the technique are presented for the one-photon transition measurement. In Section 4 the experimental results obtained in the K ($4s$–$4p$ ($^2P_{1/2}$, $^2P_{3/2}$)) are presented. Finally in Section 5, we present the results of the two-photon transition measurement performed in Cs ($6s$–$7d$ ($^2D_{3/2}$, $^2D_{5/2}$)).

2 Experimental set-up

A detailed description of the experimental set-up has already been given elsewhere [45]. The set-up combines an atomic (potassium, caesium) supersonic beam machine with a femtosecond laser system (see Fig. 1). A sequence of two ultrashort laser pulses is produced in a Michelson type interferometer. The ions, generated by the interaction between the two-pulse sequence and the atoms, are detected by a quadrupole mass spectrometer as a function of the time delay between the two pulses.

The laser system consists of a passively modelocked Titanium-Sapphire oscillator. The oscillator provides Fourier transform limited ultrashort pulses of 110 fs (FWHM) and 13 nJ. The laser spectral bandwidth (FWHM) is 8 nm or 135 cm^{-1}. The Michelson interferometer splits each pulse in two time-delayed and phase correlated pulses. On one arm of the interferometer a

hollow retroreflector mounted on a translation unit provides 6.67 fs delay steps. A pair of two plates mounted at Brewster incidence is set in the other arm of the interferometer. Counter rotation of the two plates around a vertical axis provides a continuous variation of the delay without walk-off of the laser beam. High temporal resolution (better than 0.3 fs) is thus achieved, allowing the scanning of complete interferograms. No phase locking technique as in Scherer *et al.* experiments [35,38] is used to stabilise the delay. Therefore the reproducibility is not sufficient to allow averaging of several scans. However, the signal to noise ratio is large enough to record the interferogram in a single scan. Copropagating pulses are focused with a 500 mm focal length lens on the atomic beam. The laser irradiance is thus of the order of 10^9 W/cm^2.

The alkali beam consists of three separately pumped chambers. The first chamber contains the alkali oven, the second chamber is used for differential pumping and the laser-atom interaction takes place in the third chamber. Typical oven temperatures are 400 °C and 500 °C for caesium and potassium respectively. The beam is seeded in argon at a pressure of 650 mbar. The mixture is expanded through a 150 μm nozzle. A 1 mm diameter skimmer and a 5 mm aperture further collimate the atomic beam. The ions resulting from the interaction with the linearly polarised laser beam are collected through ion optics and fed to a quadrupole mass spectrometer.

3 Theory of temporal coherent control in one-photon transitions

3.1 Introduction

Weak field interaction between an ultrashort laser pulse and a quantum system can be described adequately by perturbation theory. For one-photon transitions, this means that the interaction varies linearly with the exciting field. Thus, the response of a quantum system to a two laser pulse sequence can be described by summing the contributions of each laser pulse or by considering directly the effect of the total laser field. Two completely different physical interpretations result. A detailed discussion of these interpretations is given in the following sections.

We consider a quantum system that consists of a ground state $|g\rangle$ (used as an energy reference) and of a set of two excited states $|e_k\rangle$ ($k = 1, 2$) of energies $\hbar\omega_k$ which can be excited from the ground state through an electric dipole allowed transition (see Fig. 2). The interaction is induced by a sequence of two identical femtosecond pulses that are truly Fourier transform limited. The spectral width of these pulses ($\Delta\omega_L \cong \tau_L^{-1}$) is large enough to populate both excited states ($|\omega_L - \omega_k| \leq \Delta\omega_L$).

The total laser field can be expressed as:

$$E_T(t) = E_1(t) + E_2(t) \tag{1}$$

with

$$E_2(t) = \beta E_1(t - \tau) \tag{2}$$

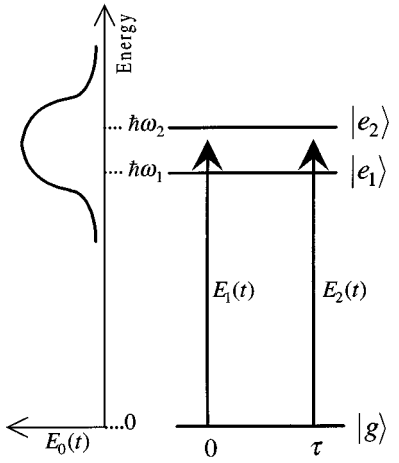

Fig. 2. Principle of the experiment. A ground state $|g\rangle$ is excited to a set of two excited states $|e_k\rangle$ (energy $\hbar\omega_k$) by a two pulse sequence. The spectral width of the two pulses is broad enough to excite simultaneously both levels (see left hand side).

and

$$E_1(t) = E_0(t)e^{-i\omega_L t} \tag{3}$$

where $E_0(t)$ represents the single pulse envelope, and τ_L and ω_L represent the pulse duration and central frequency respectively. The values β and τ are assigned to the amplitude ratio and the time delay between the two pulses respectively. In the low field regime, using the rotating wave approximation (RWA), the excited state wave function can be written as

$$|\psi(t)\rangle = \sum_k \sum_{p=1,2} \frac{i}{\hbar}\mu_{kg} \int_{-\infty}^{t} E_p(t')e^{i\omega_k(t'-t)}dt'|e_k\rangle \tag{4}$$

where μ_{kg} is the transition dipole moment from state $|g\rangle$ to state $|e_k\rangle$.

The total amplitude of the excited state $|e_k\rangle$, after interaction with the two laser pulses is written as

$$b_k(\tau) = a_k^{(1)} + a_k^{(2)}(\tau) = a_k^{(1)}(1 + e^{i\omega_k\tau}) \tag{5}$$

where $a_k^{(p)}$ is the transition probability amplitude from the ground state $|g\rangle$ towards the excited state $|e_k\rangle$ after interaction with the single pulse p ($p = 1, 2$):

$$a_k^{(p)} = \frac{i}{\hbar}\mu_{kg}\tilde{E}_p(\omega_k) \tag{6}$$

and $\tilde{E}_p(\omega_k)$ is the Fourier transform of the p pulse electric field. Throughout Sections 3.2 to 3.5, we assume that the observed signal is proportional to the total population in the excited state

$$n(\tau) = \sum_k n_k(\tau) = \sum_k |b_k(\tau)|^2 \tag{7}$$

where $n_k(\tau)$ is the population in the excited state $|e_k\rangle$ after the two pulse sequence.

3.2 Beats between quantum interferences. Ramsey fringes

The population $n_k(\tau)$ in each excited state $|e_k\rangle$ contains contributions from both laser pulses. These contributions add coherently and quantum interferences result. The relative phase $\omega_k\tau$ between the two paths (Eq. (5)) results simply from the parallel evolution of the two components of the wave function on the ground state and on the excited state during the time delay τ. Control of the excitation probability can be achieved by applying external fields to shift the energy levels $\hbar\omega_k$. More conveniently this control can be adjusted using the delay time τ. As a result, the population in the excited state $|e_k\rangle$ oscillates thus at the angular frequency ω_k. These interferences can be used to control excitation yield and to determine the transition angular frequency ω_k (see Sect. 3.4).

This scheme presents many analogies with Ramsey fringes experiments [32–34]. However, in such experiments, special care must be taken in the phase relationship between the two laser pulses in order to keep the central fringe centred on the transition frequency. Ramsey fringes are usually used to improve spectroscopic measurements when the experimental spectral linewidth is limited by the interaction time. The use of two interaction zones can improve the resolution up to the reciprocal of the time interval between the two interactions. However, this improvement is only significant when the laser bandwidth is small enough compared to these two widths. When the interaction time and thus the spectral resolution is determined by the laser pulse duration, no improvement in the resolution can be gained by adding a second interaction zone. This last case is usual in experiments with ultrashort pulses. However, recording the interferogram as a function of the time delay and measuring the oscillation frequency provides a resolution linked to the atomic linewidth (including all sources of inhomogenous broadening) but not limited by the laser bandwidth. Consequently, temporal coherent control and Ramsey fringes appear not only complementary because of the scanned parameter (temporal delay or laser frequency) but also with respect to the spectral properties of the laser source.

The total population $n(\tau)$ of the excited state manifold is the superposition of the interference pattern (interferogram) associated with the various excited states $|e_k\rangle$. Each interferogram is characterised by its own frequency ω_k. All of these frequencies lie within the spectral bandwidth $\Delta\omega_L$ of the laser frequency ω_L and as a result, the population $n(\tau)$ presents a high frequency of oscillation close to the laser frequency ω_L. These oscillations are modulated by low frequency beats at the various relative frequencies $\omega_{kk'}$ which are of the order of (or smaller than) the laser spectral width $\Delta\omega_L$, so that the period of these beats is longer than the pulse duration.

The derivation made in this section is acceptable because the various excitation channels are independent in the low field regime. This is no longer the case at higher intensities where perturbation theory is no longer valid. Depletion of the ground state induces couplings between the various excitation channels [58].

3.3 Frequency interpretation

The problem can be approached by considering the total laser field created by the two pulse sequence. This is a valid approach because the interaction is linear with respect to the laser field. After extinction of the second pulse, the total excited state wave function can be written as a function of the Fourier transform of the electric field:

$$|\psi(t)\rangle = \sum_k \frac{i}{\hbar}\mu_{kg}\tilde{E}_T(\omega_k)e^{-i\omega_k t}|e_k\rangle \tag{8}$$

and the corresponding population is

$$n(\tau) = \sum_k \left(\frac{\mu_{kg}}{\hbar}\right)^2 S(\omega_k) \tag{9}$$

where

$$S(\omega) = |\tilde{E}_T|^2 = |\tilde{E}_1|^2|1+\beta e^{i\omega\tau}|^2 \tag{10}$$

represents the intensity spectrum of the total laser field. This spectrum has the same envelope as the spectrum of a single pulse but is modulated due to optical interferences. The fringe spacing is $1/\tau$. It should be noted that this modulated spectrum is an intrinsic property of the two pulse sequence. However these optical interferences cannot be observed unless a temporal and spatial superposition of the two pulses is induced. This is for instance the case in a spectrometer where the dispersion induced by the grating stretches the pulses so that they overlap and interfere. However, if a simple detector (such as a photodiode) is used to detect the two pulse sequence, no interference is observed (the total signal is the sum of the signals resulting from each pulse independently), unless the two pulses overlap temporally. In this last case, optical interferences result in a variation of the total intensity as a function of the time delay. In our experiment, the atom behaves as a spectrometer with several slits, each one placed at one absorption frequency ω_k. The first pulse excites an atomic dipole which keeps the memory of the optical phase. The second pulse interacts with this oscillating dipole, and interferences result. The main difference with the spectrometer is that the atom induces interferences only at its absorption frequencies whereas the interferences in the spectrometer are present at all the frequencies contained in the spectrum of the pulse. The resolution is limited here by the atomic linewidth and is in general much better than the spectrometer resolution.

Expression (9) indicates that the excitation probability for each transition ($|g\rangle \rightarrow |e_k\rangle$) is proportional to the intensity spectrum at the corresponding frequency ω_k. No temporal resolution is involved here. To be valid this expression requires only that the two laser pulses are coherent with respect to each other. This relative coherence is achieved by generating the two pulse sequence from the same laser source. It can only be affected by instabilities in the delay lines. No intrinsic coherence of the initial laser pulse is necessary as evidenced by the observation of such quantum interferences using incoherent light sources [59,60].

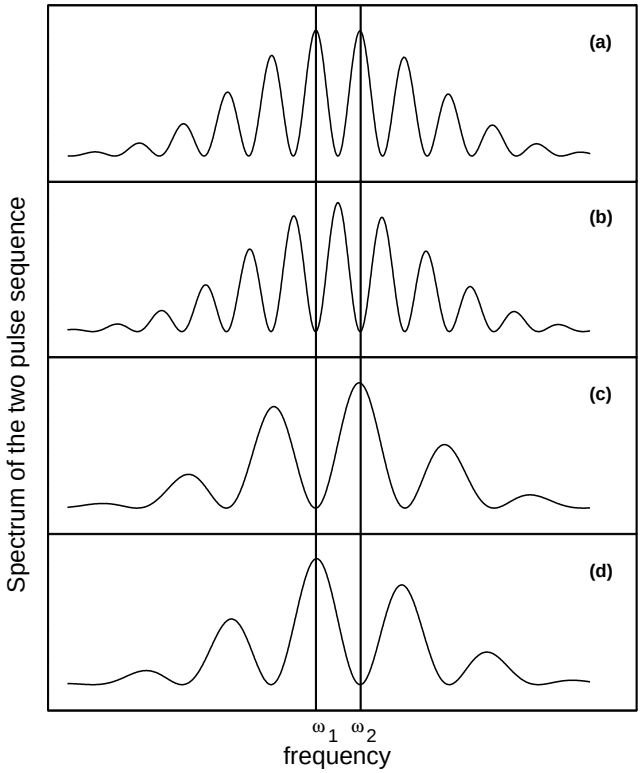

Fig. 3. Spectrum of the two pulse sequence for different values of τ. (a) and (b): the modulation spacing is equal to the excited state energy splitting; (c) and (d): the modulation spacing is equal to twice the excited state energy splitting (a) $\tau = n2\pi/\omega_1 \cong 2\pi/\Delta\omega$: to each excitation frequency corresponds a maximum in the spectrum. (b) $\tau = (n+1/2)2\pi/\omega_1 \cong 2\pi/\Delta\omega$: to each excitation frequency corresponds a minimum in the spectrum. (c) $\tau = n2\pi/\omega_2 \cong \pi/\Delta\omega$. (d) $\tau = (n+1/2)2\pi/\omega_2 \cong \pi/\Delta\omega$. In (c) and (d), the time delay is such that the spectrum has a maximum for one transition and minimum for the other transition.

The time delay dependence of the excited state population reproduces simply the dependence of the total field spectrum at the absorption frequencies ω_k of the system. When the time delay is scanned, the interference fringes scroll. The same oscillations can be observed by recording the output of a spectrometer at a fixed frequency ω_k. Ideally, the spectral resolution of the spectrometer should be adjusted to the atomic linewidth. In any case, the amplitude of oscillations decreases whenever the fringe spacing is comparable to the spectral resolution of the spectrometer, or to the atomic linewidth. For homogenous broadening, this corresponds to an excited state coherence time comparable to the time delay. For inhomogenous broadening, the frequencies associated to various "categories" of atoms result in a scrambling of the associated interferograms when the time delay is of the order of or greater than the reciprocal of the spectral linewidth. This has for instance been observed in molecules which are present in the sample in various initial rovibrational states [45].

The effects of the delay time on the spectrum are illustrated in Figure 3. This shows the spectrum of the two pulse sequence for several values of the delay time τ. The large envelope corresponds to the spectrum of a single pulse. It is modulated by oscillations of $2\pi\tau^{-1}$ period that result from interferences between the two pulses. Clearly, the delay time affects the spectrum. In Figure 3a and 3b, the delay time equals the time period associated with the excited state energy spacing ω_{21}. This means that the spacing between consecutive maxima is close to the frequency splitting. Figure 3a shows that the interference is simultaneously constructive at both ω_1 and ω_2 and as a result, the absorption probability is maximum. In contrast, Figure 3b shows the spectrum for a time delay shifted by half an optical period (approx. 1.3 fs in our case). The interference is now destructive at ω_1 and ω_2 and the absorption probability is now minimum. For values of the delay time around $\tau \approx T$, the spacing of the oscillations changes only slightly, but the maxima of the spectrum scroll with respect to the positions of the absorption frequencies. This results in oscillations of the excitation probability with the highest amplitude. On a longer time scale, the variation of the spacing between maxima becomes significant. This means that the resonance condition can be less and less simultaneously fulfilled for all the transitions: the contrast of the interference pattern decreases. When the delay time equals twice the period, the modulation spacing is half the excited state energy splitting, so that the resonance condition can be again simultaneously fulfilled for both levels and the contrast of the oscillations is maximum. This happens for each multiple of the excited state oscillation period. For delay times that fall between these cases of maximum contrast, the relative frequency excited state energy splitting ω_{21} is not a multiple of the spacing between the maxima in the spectrum. This is shown in Figures 3c and 3d which have been drawn for a delay time equal to half the oscillation period. Clearly, the spacing between consecutive maxima is twice the value of Figures 3a and 3b. If the time delay is such that the spectrum has a maximum for one transition, then it has a minimum for the other transition. For transitions of identical oscillator strengths, the overall transition probability is the same in both cases as in any other intermediate case. Therefore, when the delay time varies around $\tau \approx T/2$, no significant variation in the excitation probability is expected.

3.4 Fourier transform spectroscopy

The total excited state population contains contributions which oscillate at the various absorption frequencies of the system ω_k as a function of the time delay τ. Therefore, taking the Fourier transform of the variation of this population as a function of the time delay provides directly the product of the absorption spectrum by the laser spectrum [42]. Indeed, the optical set-up used to generate the two pulse sequence is exactly identical to those used in conventional absorption Fourier transform spectroscopy [61]. In the low intensity one-photon transition regime, it is not necessary to use coherent laser sources. Advantages of coherent over incoherent laser sources in multiphoton transitions is discussed in Section 4.

3.5 Wave packets interferences

The excited wave function (Eq. (4)) can be written as the sum of two wave packets created by each laser pulse p:

$$|\psi(t)\rangle = \sum_{p=1,2} |\psi_p(t)\rangle = \sum_{p=1,2} \left(\sum_k a_k^{(p)}(\tau) e^{-i\omega_k t} |e_k\rangle \right). \tag{11}$$

Each pulse creates a wave packet $|\psi_p(t)\rangle$ as a superposition of stationary states. The wave packet $|\psi_1(t)\rangle$ created by the first pulse evolves freely between the two laser pulses, and then interferes with the second wave packet $|\psi_2(t)\rangle$.

The time evolution of $|\psi_1(t)\rangle$ can be easily depicted using the analogy with bright states and dark states. For laser pulses short enough, we can separate the excitation step from the time evolution of the wave packet $|\psi_1(t)\rangle$. The wave packets $|\psi_1(t)\rangle$ and $|\psi_2(t)\rangle$ are therefore created in the bright state

$$|\psi_B\rangle = \cos\theta |e_1\rangle + \sin\theta |e_2\rangle \tag{12}$$

with $\tan\theta = \mu_{2g}/\mu_{1g}$. This bright state corresponds to the linear combination of excited states having the highest coupling with the ground state *via* an electric dipole transition. All linear combinations of excited states orthogonal to the bright state are not coupled to the ground state by the electric field because of destructive interferences between their various components. They are therefore named dark states. In the case of a two level system, the single dark state can be written as:

$$|\psi_D\rangle = \sin\theta |e_1\rangle - \cos\theta |e_2\rangle. \tag{13}$$

Free evolution of $|\psi_1(t)\rangle$ corresponds to an oscillation between the bright and the dark states under the effect of the free Hamiltonian of the system that couples them. The period of oscillation is again $T = 2\pi/\omega_{21}$.

The interference efficiency depends only on the overlap between $|\psi_1(\tau)\rangle$ and the second wave packet created in the bright state, $|\psi_2(\tau)\rangle = |\psi_B\rangle$. If the first wave packet is in the dark state when the second wave packet is created, no interference can take place. On the other hand, if the first wave packet is in the bright state when the second wave packet is created, then the interference takes place with the highest contrast. Therefore, the variation of the contrast of the interferences reflects the oscillation of the excited state wave packet. This technique provides similar information as pump-probe techniques on the wave packet evolution. However, the conditions to fulfil in order to observe such wave packet motions are different. For these both methods, several excited states must be populated simultaneously by the first pulse in order to create a wave packet. In the temporal coherent control method, the second transition has the same requirements as the first one. They are thus automatically fulfilled. The only constraint is to keep the transitions in the low field regime [58]. In the pump-probe method, the probe step must also satisfy the condition that its probability depends on the wave packet evolution.

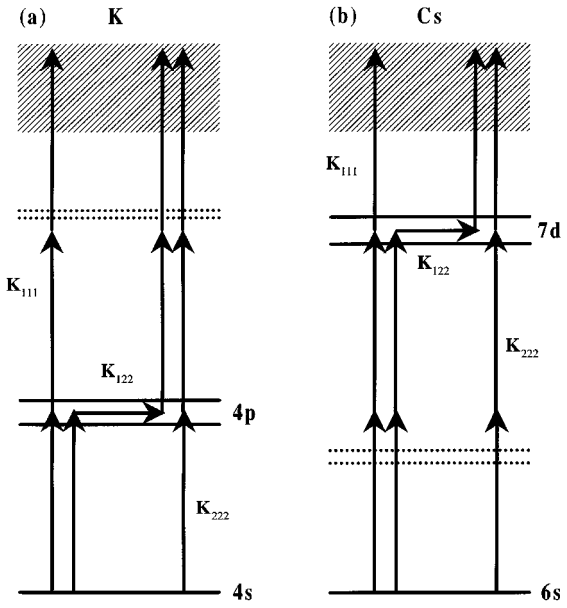

Fig. 4. Detailed scheme of energy levels and quantum paths in the two experiments. a) K ($4s$–$4p$ ($^2P_{1/2}$, $^2P_{3/2}$)) one-photon excitation followed by two-photon ionisation. b) Cs ($6s$–$7d$ ($^2D_{3/2}$, $^2D_{5/2}$)) two-photon excitation followed by one-photon ionisation. Path K_{ijk} correspond to absorption of one photon of pulse i for the first transition, of pulse j for the second transition and of pulse k for the third transition.

4 Experimental results and discussion

4.1 Ion detection

The experiment was performed in the ($4s$–$4p$) transition in potassium atoms, using a 110 fs laser operating at 769 nm. The two fine structure exited states ($4p$ ($^2P_{1/2}$, $^2P_{3/2}$), $\omega_{21} = 57.72$ cm^{-1}) are simultaneously excited by the two pulse sequence (Fig. 4a). The excited state population is detected by two photon ionisation that occurs within the two laser pulses. The amplitude ratio between the two laser pulses is $\beta \approx 1.4$.

For delay times larger than the pulse duration, three quantum paths to ionisation are possible:

- K_{111} (or K_{222}) when both the excitation and the ionisation take place within the first pulse (second pulse respectively)
- K_{122} when the excitation is induced by the first pulse and the two photon ionisation performed by the second pulse.

If the two pulses overlap, eight paths K_{ijk} (with $i, j, k = 1, 2$) are possible. First, we discuss the case of separate laser pulses. The ion signal

$$S_I = |K_{111} + K_{122} + K_{222}|^2 \tag{14}$$

contains contributions $|K_{ijk}|^2$ from each separate path and crossed terms corresponding to interferences between these various paths. However, the interference term associated to paths producing ions at times separated by the delay time τ (path K_{111} on the one hand, and paths K_{122}

and K_{222} on the other hand) vanishes. Indeed, the emitted electron has a kinetic energy distribution comparable to the laser spectral width $\Delta E \approx \hbar\Delta\omega_L$. Therefore, the corresponding phase shifts $\Delta E\tau\hbar$ between electrons emitted by the two pulses cover completely an interval much larger than $[0; 2\pi]$ and the interference contribution vanishes after averaging over the kinetic energy distribution of the ejected electron. This result can also be understood by realising that destructive interferences would imply that the electron ejected by the first pulse could be recombined with the ion by the second pulse, even after a long delay, which is not realistic. The total ion signal is therefore given by

$$S_I = |K_{111}|^2 + |K_{122} + K_{222}|^2. \quad (15)$$

The term $|K_{111}|^2$ corresponds to the contribution from the first pulse alone and is independent of the time delay τ. The term $|K_{122}+K_{222}|^2$ contains the interference between the two paths leading to the excitation of the $4p$ state by the first or the second pulse. This interference is displayed on the ion signal induced by the second pulse. The behaviour of $|K_{122} + K_{222}|^2$ as a function of time delay is qualitatively similar to that of the excited state population given by equation (7) or (9). The only difference is that in path K_{222}, the excited state population is created and probed simultaneously by the same laser pulse. This reduces the probe efficiency by approximately a factor of 2 compared to path K_{122}. This double role of the second laser pulse reduces the contrast of the interferences by approximately a factor of 2, but does not change its qualitative features.

During the time overlap of the two laser pulses, optical interferences occur before the interaction with the atoms. The laser intensity integrated over time depends on the phase of this interference. Thus, the excitation probability and the ion signal reflect directly the variations in laser intensity. For $|\tau| \ll \tau_L$, the ion signal is easily calculated by assuming proportional amplitudes for the two pulses:

$$S_I = |K_{111}|^2|1 + \beta e^{i\omega_L\tau}|^6. \quad (16)$$

This results in large amplitude oscillations between the minimum $(1-\beta)^6$ and the maximum $(1+\beta)^6$ with a large asymmetry (when β is of the order of unity) between constructive and destructive interferences with respect to the "incoherent" case when the effect of the two pulses add independently, $(1+\beta^6)$. Moreover, these optical interferences occur at the central laser frequency ω_L, slightly different from the frequencies ω_k at which the quantum interferences oscillate. However, this difference is too small to be measured since the number of periods of the optical interferences is of the order of $\omega_L\tau_L$, smaller than $\omega_L/(\omega_L-\omega_k)$.

4.2 Results

The experimental results of the one-photon interference case are shown on Figure 5. A long range scan ([−2 ps; +16 ps]) was obtained with the low resolution device (6.67 fs steps). The rapid oscillations (period of 2.6 fs) are largely undersampled, but can still be detected. They are modulated by slow oscillations of 580 fs period the reciprocal of the energy spacing between the two fine structure excited states (see Sect. 3.4). These slow oscillations result from one of the following: (*i*) beats between the interferograms associated with the two excited states (see Sect. 3.2), (*ii*) the modulated spectrum of the two pulse sequence (see Sect. 3.3), (*iii*) the wave packet oscillations between the bright state and the dark state (see Sect. 3.5). As discussed in Section 4.1, when the laser pulses overlap, optical interferences produce a strong peak around zero delay. The large asymmetry between constructive and destructive interferences shows up clearly as predicted by equation (16).

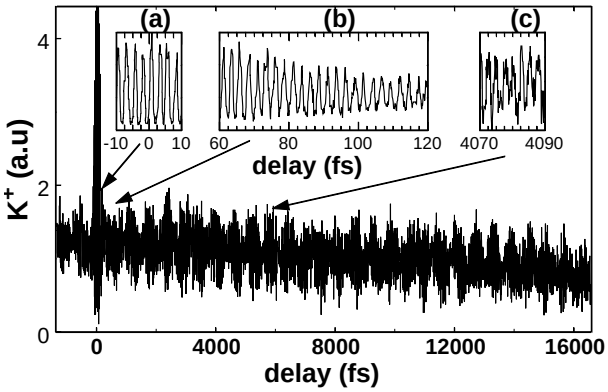

Fig. 5. Coherent control in potassium atoms. Excitation of the $4s-4p$ transition at $\lambda = 769$ nm at low resolution (6.67 fs). Insets show extended views at high resolution (0.3 fs) in the optical interferences region (a), in the quantum interferences region (b) and of the transition from optical interferences to quantum interferences (c). The fast oscillation has in all cases a period of ca 2.56 fs.

Figure 5 displays also three insets with fine scanning of parts of the interferogram obtained with the high resolution device (0.3 fs resolution). Insets 5a and 5c correspond to short and long time delays respectively. They are associated to the optical interferences (total pulse overlap) and to the quantum interferences (no pulse overlap) respectively. Inset 5b shows also the transition region when the pulses overlap partially. In the three cases, the oscillation period is about 2.56 fs. This period corresponds to the optical period at 769 nm as well as to the average Bohr frequency of the two ($4s-4p$ ($^2P_{1/2}$, $^2P_{3/2}$)) transitions. The two types of interferences cannot be distinguished. However the oscillation amplitude is symmetric in the case of quantum interferences since these interferences arise in a one-photon process (the $4s-4p$ transition) and are largely asymmetric in the case of optical interferences which involve a three photon process.

4.3 Discussion

In the particular case of a fine structure multiplet, the bright state and the dark state have a straightforward interpretation. Since the electronic spin is not affected by an electric dipole transition, and the two fine structure excited states can be simultaneously excited, it is appropriate to use the uncoupled $|l, m_l, s, m_s\rangle$ basis set. The results are independent of the initial orientation of the electronic spin and as an example and for simplicity, we assume that the ground state is in an eigen vector of S_z, $|m_l = 0, m_s = 1/2\rangle$. In case of linear polarisation along the Oz axis, the bright state prepared by an ultrashort excitation is $|m'_l = 0, m'_s = 1/2\rangle$. This state is not an eigen state of the free atom Hamiltonian. It is coupled to the dark state $|m'_l = 1, m'_s = -1/2\rangle$ by the spin-orbit Hamiltonian. This coupling produces the oscillation between the bright state and the dark state during the free evolution of the system after excitation by the first pulse, at a period which is the reciprocal of the coupling strength in the uncoupled basis set or of the energy splitting in the coupled basis set. This oscillation corresponds classically to the precession of the electronic spin and of the orbital angular momentum along the total angular momentum vector.

We have shown in Sections 3 and 4 that in one photon two pulses experiments, temporal Ramsey fringes result from quantum interferences. Due to the linearity of the interaction, these experiments can be equivalently described in the temporal or spectral domain. In the time domain, two wave packets are excited at two different times and quantum interferences result. In the spectral domain, the modulated spectrum of the two pulse sequence explains the observed data. Moreover, we have seen that the non-linearity in the detection step results in large amplitude oscillations due to optical interferences while the laser pulses overlap. The quantum interferences have a frequency close to the mean laser frequency ω_L, the natural frequency of the optical interferences. In summary, for an one-photon transition, the quantum and optical interferences are indistinguishable by their frequencies. However, this aspect does not change the capacity to control the excitation cross section.

In the next section, we present the case of temporal coherent control in a two photon transition where optical and quantum interferences are clearly distinguished [43].

5 Wave packet interferences in two photon transitions

Theoretical and experimental investigations of wave packet interferences induced by a two-pulse sequence in a two-photon transition have already been reported [43]. In this section, we present their main features with a particular emphasis on their differences with one photon transitions. Figure 4b shows the atomic system used to illustrate this case. A Ti:sapphire laser operating at 768 nm is used to excite Cs by a two-photon transition, ($6s$−$7d$ ($^2D_{3/2}$, $^2D_{5/2}$)). Both $7d$ doublet states can be simultaneously reached because the laser bandwidth is much wider than the 20.97 cm^{-1} fine structure splitting. The interferences created by the two-pulse sequence are detected with a one-photon ionisation step induced by the same laser pulses.

5.1 Theory

The atomic system consists of three sets of levels: ground state $|g\rangle$, intermediate states $|i_m\rangle$, and excited states $|e_k\rangle$ ($k = 1,\ 2$) of energies 0, $\hbar\omega_m$, and $\hbar\omega_k$ respectively. Transitions from the ground state to the intermediate states and from the intermediate states to the excited states are considered electric dipole allowed. We assume resonant two-photon transition ($|g\rangle \rightarrow |e_k\rangle$) with all the excited states ($|2\omega_L - \omega_k| \leq \Delta\omega_L$) and non-resonant one-photon transition. with the intermediate states ($|\omega_m - \omega_L| \gg \Delta\omega_L$).

The two-photon transition is equivalent to a one-photon transition with an effective dipole moment given by the two-photon transition operator [62]

$$Q_{kg} = \sum_m \frac{\langle e_k|\mu|i_m\rangle\langle i_m|\mu|g\rangle}{\hbar(\omega_m - \omega_L)} \tag{17}$$

and an effective field E^2_{tot}. Using equation (4) or (8), the wave packet amplitude $b_k(\tau)$ in the excited state $|e_k\rangle$ can be written as

$$b_k(\tau) = a_k^{(11)} + a_k^{(22)}(\tau) + 2a_k^{(12)}(\tau) \tag{18}$$

with

$$\begin{aligned} a_k^{(11)} &= \frac{i}{\hbar} Q_{kg} e^{-i\omega_k t} \tilde{E}_0^2(\omega_k - 2\omega_L) \\ a_k^{(22)}(\tau) &= \beta^2 a_k^{(11)} e^{i\omega_k \tau} \\ a_k^{(12)}(\tau) &= \frac{i}{\hbar} Q_{kg} \beta e^{-i\omega_k \tau} e^{i\omega_L \tau} \\ &\quad \times \int_{-\infty}^{+\infty} E_0(t') E_0(t' - \tau) e^{i(2\omega_L - \omega_k)t'} dt' \end{aligned} \tag{19}$$

where $\tilde{E}_0^2(\omega)$ is the Fourier transform of the square of single pulse electric field. The amplitude $a_k^{(ij)}(\tau)$ corresponds to absorption of one photon from pulse (i) and one photon from pulse (j). The crossed term $a_k^{(12)}(\tau)$ is significant only when the pulses overlap ($|\tau| \leq \tau_L$) because none of the laser pulses is resonant with any intermediate state.

It is important to call attention to the difference between the Fourier transform of the square of the field and the square of the Fourier transform of the field. Indeed, this difference implies that the intensity spectrum of the two pulse sequence does not play any role in understanding the time delay dependence of the excitation probability. The population in state $|e_k\rangle$, $n_k(\tau)$, as well as the total population $n(\tau)$, include contributions from each of the three paths $|a_k^{(ij)}(\tau)|^2$ taken individually, and the crossed terms corresponding to interferences between these various paths.

All the qualitative features of the quantum interferences in a two-photon interaction can be derived from two

simple cases: (1) total overlap of the pulses ($|\tau| \ll \tau_L$), and (2) complete separation ($|\tau| \gg \tau_L$). A detailed discussion of these two cases follows.

For $|\tau| \ll \tau_L$, the two pulses interfere optically before interacting with the atom. Their amplitudes are proportional and their phases differ by $\omega_L\tau$. The total field reduces to

$$E_T(t) = (1 + \beta e^{i\omega_L\tau})E_0(t). \tag{20}$$

The population in the excited state $|e_k\rangle$ after the interaction becomes

$$n_k(\tau) = |a_k^{(11)}|^2|1 + \beta e^{i\omega_L\tau}|^4. \tag{21}$$

This population oscillates as a function of τ at the laser frequency ω_L. The ion signal, which results from absorption of a third photon from the same laser sequence, also oscillates at the same frequency and can be expressed as

$$S'_I = |K'_{111}|^2|1 + \beta e^{i\omega_L\tau}|^6 \tag{22}$$

which is similar to the (1+2) photon case studied in Section 4 (see Eq. (16)).

For $|\tau| \gg \tau_L$, the amplitude $a_k^{(12)}(\tau)$ vanishes. The excited state population takes again a simple expression:

$$n_k(\tau) = |a_k^{(11)}|^2|1 + \beta^2 e^{i\omega_k\tau}|^2. \tag{23}$$

This population oscillates at the excitation frequency as in the one-photon transition case (see Eqs. (6) and (7)). However, this frequency is now twice the laser frequency, providing a direct distinction between the optical interferences and the quantum interferences.

The discussion presented in Section 4.1 is still valid for the ion signal because it is generated from contributions arising from pulses (1) and (2). Ionisation due to pulse (1) produces a signal independent of the delay time. Pulse (2) ionises the excited state population produced by the combination of pulses (1) and (2) and the resulting signal contains the quantum interferences described by equation (23).

5.2 Experimental results and discussion

The experiment was performed with laser pulses of equal intensity ($\beta \approx 1$).The experimental results are displayed in Figure 6. The general features are the same as those observed in the one-photon transition case (see Fig. 5): large amplitude oscillations in the region of pulse overlap ($|\tau| \leq \tau_L$) where optical interferences dominate; beats (of 1.59 ps) between the two excited states interference patterns when the quantum interferences are present ($|\tau| \geq \tau_L$). The major difference with the one-photon case shows up clearly in the three high resolution insets. Inset 6a (for $|\tau| \ll \tau_L$) shows the optical interferences with a period of 2.56 fs. Inset 6c (for $|\tau| \gg \tau_L$) shows the quantum interferences with a period of 1.28 fs. Inset 6b (for $|\tau| \cong \tau_L$) shows the transition between the two regimes. One part of the laser sequence contributes to optical interferences,

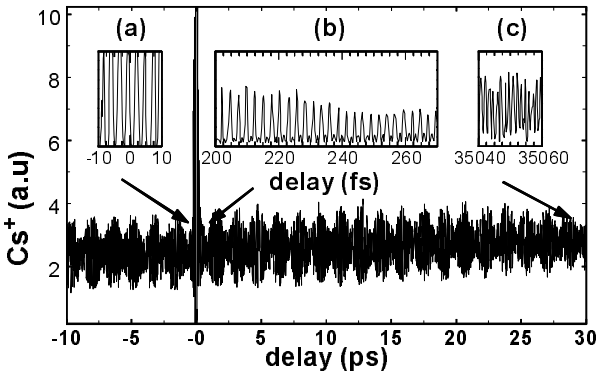

Fig. 6. Coherent control in caesium atoms. Excitation of the $6s{-}7d$ transition at $\lambda = 768$ nm at low resolution (6.67 fs). Insets show extended views at high resolution (0.3 fs) in the optical interferences region (a), in the quantum interferences region (b) and of the transition from optical interferences to quantum interferences (c). The fast oscillation has a period of 2.56 fs for optical interferences, 1.28 fs for quantum interferences.

while the other produces interfering wave packets. As the delay time increases, the contribution of the wave packet interferences increases and the second harmonics pattern grows in the interferogram.

Among the interpretations given in Section 3, the quantum interferences interpretation (viewed as wave packet interferences or as interferences in each eigenstate) are still valid. The spectral interpretation however is no longer valid since the excitation amplitude is a quadratic function of the electric field. This technique can also be used as a Fourier transform spectroscopy (FTS) technique [44]. For this investigation, it presents a major advantage compared to standard FTS due to the high peak intensity available with coherent ultrashort pulses. The technique can also be used to access states of the same symmetry as the ground state.

6 Conclusion

We have described a theoretical and experimental investigation of temporal coherent control in atomic one-photon and two-photon transitions. This temporal coherent control is based on interferences of two wave packets produced by a sequence of two identical ultrashort laser pulses. The overlap between the two wave packets governs the contrast of the resulting oscillations and their relative quantum phase defines the constructive or destructive behaviour of the interferences. They are detected by ionisation of the atom within the laser pulse sequence.

We have clearly demonstrated the relationship and the differences between quantum interferences and optical interferences. These optical interferences take place when the laser pulses overlap. They produce variations of the incident laser power when the interference phase is scanned. Because of the nonlinearity of the overall process, the optical interferences result in strong asymmetric variations of

the ion signal. On the other hand, quantum interferences between both excitation paths take place when the laser pulses are well separated. They result from a linear superposition of both quantum wave packets. The corresponding variations are symmetric. Another feature differentiates these two kinds of interferences. Their characteristic frequency is the transition frequency for the quantum interferences and the mean laser frequency for the optical interferences. If these two frequencies are not easily distinguishable in the case of one-photon transitions, they differ by a factor of two in the case of two-photon transitions, so that they can be clearly identified.

In the case of one-photon transitions at low laser intensity, the linear relationship between the excited state wave function and the electric field allows several complementary interpretations of the same phenomenon. Beats of quantum interferences and wave packet interferences have thus been described and analysed. These two interpretations remain valid in two-photon transitions. In one-photon transitions, the system response can also be interpreted in terms of the spectral content of the two pulse sequence. However, this analogy can be misleading since it implicitly implies an interaction between the two pulses before interaction with the atom, which is not the case. Finally, the response of the system suggests that this interaction scheme can be applied to Fourier transform spectroscopy. The high power density available in ultrashort pulses makes it possible to extend Fourier transform spectroscopy to multiphoton transitions.

This experiment is comparable to a two-slit experiment where each slit is associated to one laser pulse [55, 56]. In the two-slit experiment, interferences occur because it is impossible to determine with certainty the slit that the particle goes through. In our experiment, interferences occur because it is impossible to distinguish between the two excitation paths. This indistinguishable condition is fulfilled only after total extinction of the two laser pulses.

The scheme presented is a simple example of coherent control of an excited state wave packet. The excited state wave packet can be either enhanced or destroyed by the second laser pulse. More interesting cases can be considered if two different channels can be simultaneously controlled. One could for instance prepare a superposition of two wave packets evolving each towards a different channel. Depending on the delay time between the two pulses, each wave packet can be controlled with a different control parameter so that the branching ratio between the two channels can be modulated.

We sincerely acknowledge G. Trénec, A. Pellicer, P. Paquier, M. Gianesin for their technical help in the building of the experiment. We enjoyed stimulating discussions with A. Beswick, B. de Beauvoir, J.P. Daudey, P. Labastie, and J. Vigué.

This work has been financially supported by the Centre National de la Recherche Scientifique (C.N.R.S.), the Ministère de l'Éducation Nationale, de l'Enseignement Supérieur et de la Recherche (M.E.N.E.S.R), the Procope program 97183, the Région Midi-Pyrénées and l'Institut Universitaire de France.

References

1. P. Brumer, M. Shapiro, Chem. Phys. Lett. **126**, 541 (1986).
2. M. Shapiro, J.W. Hepburn, P. Brumer, Chem. Phys. Lett. **149**, 451 (1988).
3. S. Shi, A. Woody, H. Rabitz, J. Chem. Phys. **88**, 6870 (1988).
4. R. Kosloff, S.A. Rice, P. Gaspard, S. Tersigni, D.J. Tannor, Chem. Phys. **139**, 201 (1989).
5. R.S. Judson, H. Rabitz, Phys. Rev. Lett. **68**, 1500 (1992).
6. W.S. Warren, H. Rabitz, M. Dahleh, Science **259**, 1581 (1993).
7. B. Kohler, V.V. Yakovlev, J. Che, J.L. Krause, M. Messina, K.R. Wilson, N. Schwentner, R.M. Whitnell, Y. Yan, Phys. Rev. Lett. **74**, 3360 (1995).
8. D.W. Schumacher, J.H. Hoogenraad, D. Pinkos, P.H. Bucksbaum, Phys. Rev. A **52**, 4719 (1995).
9. A. Assion, T. Baumert, J. Helbing, V. Seyfried, G. Gerber, Chem. Phys. Lett. **259**, 488 (1996).
10. C.J. Bardeen, J. Che, K.R. Wilson, V.V. Yakovlev, P. Cong, B. Kohler, J.L. Krause, and M. Messina, J. Phys. Chem. A **101**, 3815 (1997).
11. E.D. Potter, J.L. Herek, S. Pedersen, Q. Liu, A.H. Zewail, Nature **355**, 66 (1992).
12. J.L. Herek, A. Materny, A.H. Zewail, Chem. Phys. Lett. **228**, 15 (1994).
13. T. Baumert, B. Bühler, R. Thalweiser, G. Gerber, Phys. Rev. Lett. **64**, 733 (1990).
14. S. Rutz, S. Greschik, E. Schreiber, L. Wöste, Chem. Phys. Lett. **257**, 365 (1996).
15. U. Gaubatz, P. Rudecki, S. Schiemann, K. Bergmann, J. Chem. Phys. **92**, 5363 (1990).
16. Y.L. Shao, D. Charalambidis, C. Fotakis, J. Zhang, P. Lambropoulos, Phys. Rev. Lett. **67**, 3669 (1991).
17. A. Shnitman, I. Sofer, I. Golub, A. Yogev, M. Shapiro, Z. Chen, P. Brumer, Phys. Rev. Lett. **76**, 2886 (1996).
18. M. Shapiro, P. Brumer, Int. Rev. Phys. Chem. **13**, 187 (1994).
19. C. Chen, Y.-Y. Yin, D.S. Elliott, Phys. Rev. Lett. **64**, 507 (1990).
20. S.M. Park, S. P. Lu, R.J. Gordon, J. Chem. Phys. **94**, 8622 (1991).
21. V.D. Kleiman, L. Zhu, X. Li, R.J. Gordon, J. Chem. Phys. **102**, 5863 (1995).
22. L. Zhu, V. D. Kleiman, X. Li, S.P. Lu, K. Trentelman, R.J. Gordon, Science **270**, 77 (1995).
23. X. Wang, R. Bersohn, K. Takahashi, M. Kawasaki, H.L. Kim, J. Chem. Phys. **105**, 2992 (1996).
24. N.E. Karapanagioti, D. Xenakis, D. Charalambidis, C. Fotakis, J. Phys. B **29**, 3599 (1996).
25. S. Cavalieri, R. Eramo, L. Fini, Phys. Rev. A **55**, 2941 (1997).
26. H.G. Muller, P.H. Bucksbaum, D.W. Schumacher, A. Zavriyev, J. Phys. B **23**, 2761 (1990).
27. Y.-Y. Yin, D.S. Elliott, R. Shehadeh, E.R. Grant, Chem. Phys. Lett. **241**, 591 (1995).
28. E. Charron, A. Giusti-Suzor, F.H. Mies, Phys. Rev. Lett. **71**, 692 (1993).
29. B. Sheehy, B. Walker, L.F. DiMauro, Phys. Rev. Lett. **74**, 4799 (1995).
30. E. Dupont, P.B. Corkum, H.C. Liu, M. Buchanan, Z.R. Wasilewski, Phys. Rev. Lett. **74**, 3596 (1995).

31. E. Charron, A. Giusti-Suzor, F.H. Mies, Phys. Rev. Lett. **75**, 2815 (1995).
32. M.M. Salour, C. Cohen-Tannoudji, Phys. Rev. Lett. **38**, 757 (1977).
33. R. Teets, J. Eckstein, T.W. Hänsch, Phys. Rev. Lett. **38**, 760 (1977).
34. C.J. Bordé, C. Salomon, S. Avrillier, A. Van Lerberghe, C. Bréant, Phys. Rev. A **30**, 1836 (1984).
35. N.F. Scherer, R.J. Carlson, A. Matro, M. Du, A.J. Ruggiero, V. Romerorochin, J.A. Cina, G.R. Fleming, S.A. Rice, J. Chem. Phys. **95**, 1487 (1991).
36. L.D. Noordam, D.I. Duncan, T.F. Gallagher, Phys. Rev. A **45**, 4734 (1992).
37. R.R. Jones, C.S. Raman, D.W. Schumacher, P.H. Bucksbaum, Phys. Rev. Lett. **71**, 2575 (1993).
38. N.F. Scherer, A.J. Ruggiero, M. Du, G.R. Fleming, J. Chem. Phys. **93**, 856 (1990).
39. V. Blanchet, M.A. Bouchene, O. Cabrol, B. Girard, Chem. Phys. Lett. **233**, 491 (1995).
40. R.R. Jones, Phys. Rev. Lett. **75**, 1491 (1995).
41. V. Blanchet, M.A. Bouchene, B. Girard, in *Fast Elementary Processes in Chemistry and Biophysics*, edited by A. Tramer (American Institute of Physics, 1996).
42. V. Blanchet, M.A. Bouchene, B. Girard, in *Femtochemistry: Ultrafast chemical and physical processes in molecular systems*, edited by M. Chergui (World Scientific, Singapore, 1996), pp. 326.
43. V. Blanchet, C. Nicole, M.A. Bouchene, B. Girard, Phys. Rev. Lett. **78**, 2716 (1997).
44. M. Bellini, A. Bartoli, T.W. Hansch, Opt. Lett. **22**, 540 (1997).
45. V. Blanchet, M.A. Bouchene, B. Girard, J. Chem. Phys. **108**, 4862 (1998).
46. J.A. Yeazell, M. Mallalieu, C.R. Stroud, Jr., Phys. Rev. Lett. **64**, 2007 (1990).
47. B. Broers, J.F. Christian, J.H. Hoogenaard, W.J. van der Zande, H.B. van Linden van den Heuvell, L.D. Noordam, Phys. Rev. Lett. **71**, 344 (1993).
48. J.F. Christian, B. Broers, J.H. Hoogenraad, W.J. Van der Zande, L.D. Noordam, Opt. Commun. **103**, 79 (1993).
49. L. Marmet, H. Held, G. Raithel, J. A. Yeazell, H. Walther, Phys. Rev. Lett. **72**, 3779 (1994).
50. J.Y. Bigot, M.-A. Mycek, S. Weiss, R.G. Ulbrich, D.S. Chemla, Phys. Rev. Lett. **70**, 3307 (1993).
51. X. Marie, P. Le Jeune, T. Amand, M. Brousseau, J. Barrau, M. Paillard, R. Planel, Phys. Rev. Lett. **78**, 3222 (1997).
52. N.F. Scherer, L.D. Ziegler, G.R. Fleming, J. Chem. Phys. **96**, 5544 (1992).
53. J. Wals, H.H. Fielding, J.F. Christian, L.C. Snoek, W.J. van der Zande, H.B. van Linden van den Heuvell, Phys. Rev. Lett. **72**, 3783 (1994).
54. O. Kinrot, I.S. Averbukh, Y. Prior, Phys. Rev. Lett. **75**, 3822 (1995).
55. H. Metiu, V. Engel, J. Opt. Soc. Amer. B **7**, 1709 (1990).
56. R. Bavli, V. Engel, H. Metiu, J. Chem. Phys. **96**, 2600 (1992).
57. V. Engel, H. Metiu, J. Chem. Phys. **100**, 5448 (1994).
58. C. Nicole, M.A. Bouchene, S. Zamith, N. Melikechi, B. Girard (in preparation).
59. R.R. Jones, D.W. Schumacher, T.F. Gallagher, P.H. Bucksbaum, J. Phys. B **28**, L405 (1995).
60. L.C. Snoek, S.G. Clement, F.J.M. Harren, W.J. van der Zande, Chem. Phys. Lett. **258**, 460 (1996).
61. M. Quack, Annu. Rev. Phys. Chem. **41**, 839 (1990).
62. B. Cagnac, G. Grynberg, F. Biraben, J. Phys. France **34**, 845 (1973).